Corrected 11 February 2020. See full text.

RESEARCH ARTICLE

CELLULAR NEUROSCIENCE

Local protein synthesis is a ubiquitous feature of neuronal pre- and postsynaptic compartments

Anne-Sophie Hafner[1]*, Paul G. Donlin-Asp[1]*, Beulah Leitch[2], Etienne Herzog[3,4], Erin M. Schuman[1]†

There is ample evidence for localization of messenger RNAs (mRNAs) and protein synthesis in neuronal dendrites; however, demonstrations of these processes in presynaptic terminals are limited. We used expansion microscopy to resolve pre- and postsynaptic compartments in rodent neurons. Most presynaptic terminals in the hippocampus and forebrain contained mRNA and ribosomes. We sorted fluorescently labeled mouse brain synaptosomes and then sequenced hundreds of mRNA species present within excitatory boutons. After brief metabolic labeling, >30% of all presynaptic terminals exhibited a signal, providing evidence for ongoing protein synthesis. We tested different classic plasticity paradigms and observed distinct patterns of rapid pre- and/or postsynaptic translation. Thus, presynaptic terminals are translationally competent, and local protein synthesis is differentially recruited to drive compartment-specific phenotypes that underlie different forms of plasticity.

Neurons are morphologically complex, comprising a typical cell body from which emerges elaborately branching dendrites and axons. Most of a neuron's area is accounted for by its dendrites and axons: For example, the dendrites of a rodent pyramidal neuron exceed 10 mm in length (*1*), and a human axon (e.g., in the sciatic nerve) can reach up to 1 m. The massive network represented by dendrites and axons provides the surface area to accommodate the 1000 to 10,000 synapses, both excitatory and inhibitory, typically formed by an individual neuron. At synapses, the complement of proteins present is the best phenotypic indicator of both the type and the strength of the synapse. The regulation of synaptic proteins, by posttranslational modifications and by ongoing protein synthesis and degradation, drives homeostasis and plasticity at synapses (*2*–*4*).

It has been proposed that a substantial fraction of proteome supply and remodeling occurs locally within synapses (*5*–*8*). Whereas a wealth of data has led to the consensus that protein synthesis occurs in mature dendrites (*7*, *9*), there has been much less agreement about local translation in mature axons. Many studies have shown that local translation is required for axonal growth during development and repair after injury [e.g., (*10*–*14*)]. In addition, a few recent studies have shown that mature retinal ganglion cell axons contain competent translational machinery and mRNAs (*15*) or use presynaptic translation during plasticity at certain synapse types (*16*, *17*). In addition, there is ample evidence that invertebrate axons can synthesize proteins [e.g., (*18*)]. Despite these data, controversy has arisen from an inability to reliably detect ribosomes in axons or terminals (*19*, *20*) and the persistent idea that axonal protein needs are adequately served by the well-documented system of axonal transport [e.g., (*21*)].

To determine whether translation in axon terminals is a common feature of mature brains, we used advanced microscopy methods to determine the abundance and diversity of the components required for translation in nerve terminals from multiple brain areas. We also purified a molecularly defined population of mature presynaptic nerve terminals and directly sequenced the resident mRNA population. Lastly, we conducted high-resolution metabolic labeling to ascertain the frequency of protein synthesis events in all synaptic compartments.

Presynaptic terminals from the cortex and hippocampus contain translation machinery

Efforts to localize molecules or cell biological events to neuronal pre- or postsynaptic compartments by using fluorescence microscopy are limited by the tight association of the axonal bouton and the dendritic spine or synapse. The synaptic cleft, the only clear region of separation, is only ~20 nm wide. To increase the resolving power to visualize RNA molecules in pre- and postsynaptic compartments, we optimized fluorescence in situ hybridization (FISH) and nascent protein detection methods for use with expansion microscopy (*22*) (Fig. 1A; see methods). In adult mouse brain slices or rat hippocampal neurons cultured for 18 to 21 days in vitro (DIV), expansion resulted in an enlargement of both pre- and postsynaptic compartments, with an average expansion of ~3.4-fold (fig. S1), yielding a clear separation between the pre- and postsynaptic compartments (movie S1). To evaluate whether ribosomes and mRNA species are present in defined presynaptic compartments, we used immunolabeling for either excitatory [vesicular glutamate transporter 1 (vGLUT1)] (*23*, *24*) or inhibitory [vesicular GABA transporter (vGAT)] (*25*, *26*) nerve terminals in expanded mouse brain sections (from both the forebrain and hippocampus) (Fig. 1, B to E, and fig.S2) or rat cultured hippocampal neurons (fig. S3). We took care to identify the molecules of interest within individual *z* sections positively labeled for excitatory or inhibitory terminals (fig. S1). Signal detected outside of immunolabeled compartments corresponded to signal arising from nearby unlabeled cells (fig. S3). We detected ribosomes in a large majority (>75%) of both excitatory and inhibitory presynaptic nerve terminals by using antibodies directed against either a small (RPS11) or a large (RPL26) ribosomal protein (Fig. 1, B to E, and figs. S2 and S4). Next, we used FISH probes to detect 18S and 28S rRNAs, as well as polyadenylated [poly $(A)^+$] mRNA {detected with a polydeoxythymidine [poly(dT)] probe}, in expanded samples (Fig. 1, B to E). Consistent with the abundance of ribosomal proteins, we detected rRNA in >80% of both excitatory and inhibitory nerve terminals (Fig. 1, B to E, and figs. S2 and S4). Ribonuclease (RNase) treatment effectively reduced all rRNA FISH signal (fig. S3). In cultured neurons, we also noted that poly $(A)^+$ mRNA was abundant, as expected, within dendritic spines (fig. S4). In addition, we used an anti-tau antibody to label axons and detected both 18S and 28S rRNAs in axonal segments (fig. S4). Thus, mRNAs and ribosomes were abundant in excitatory and inhibitory presynaptic nerve terminals.

Isolation and characterization of vGLUT1$^+$ terminals from the adult mouse brain

The presence of ribosomes and poly $(A)^+$ mRNA in axon terminals suggested the capacity for protein synthesis but did not indicate the mRNA population potentially available for translation in identified synapse types. To characterize transcripts and translational machinery in excitatory presynaptic terminals, we used our recently developed platform that couples fluorescence sorting with biochemical fractionation to sort and purify fluorescently labeled synaptosomes [fluorescence-activated synaptosome sorting (FASS)] (Fig. 2A and fig. S5). The "presorted" and sorted synaptosomes constitute resealed presynaptic and synaptic compartments, sometimes associated with an "open" postsynaptic membrane (*27*–*29*) (Fig. 2B). The sorted synaptosomes also lacked dendritic and endoplasmic reticulum (ER) elements (fig. S6). Starting with the forebrain of adult vGLUT1^{VENUS}

[1]Max Planck Institute for Brain Research, Frankfurt, Germany. [2]Department of Anatomy, School of Biomedical Sciences and the Brain Health Research Centre, University of Otago, Dunedin, New Zealand. [3]Interdisciplinary Institute for Neuroscience, University of Bordeaux, UMR 5297, F-33000, Bordeaux, France. [4]Interdisciplinary Institute for Neuroscience, CNRS, UMR 5297, F-33000, Bordeaux, France.
*These authors contributed equally to this work.
†Corresponding author. Email: erin.schuman@brain.mpg.de

Corrected 11 February 2020. See full text.

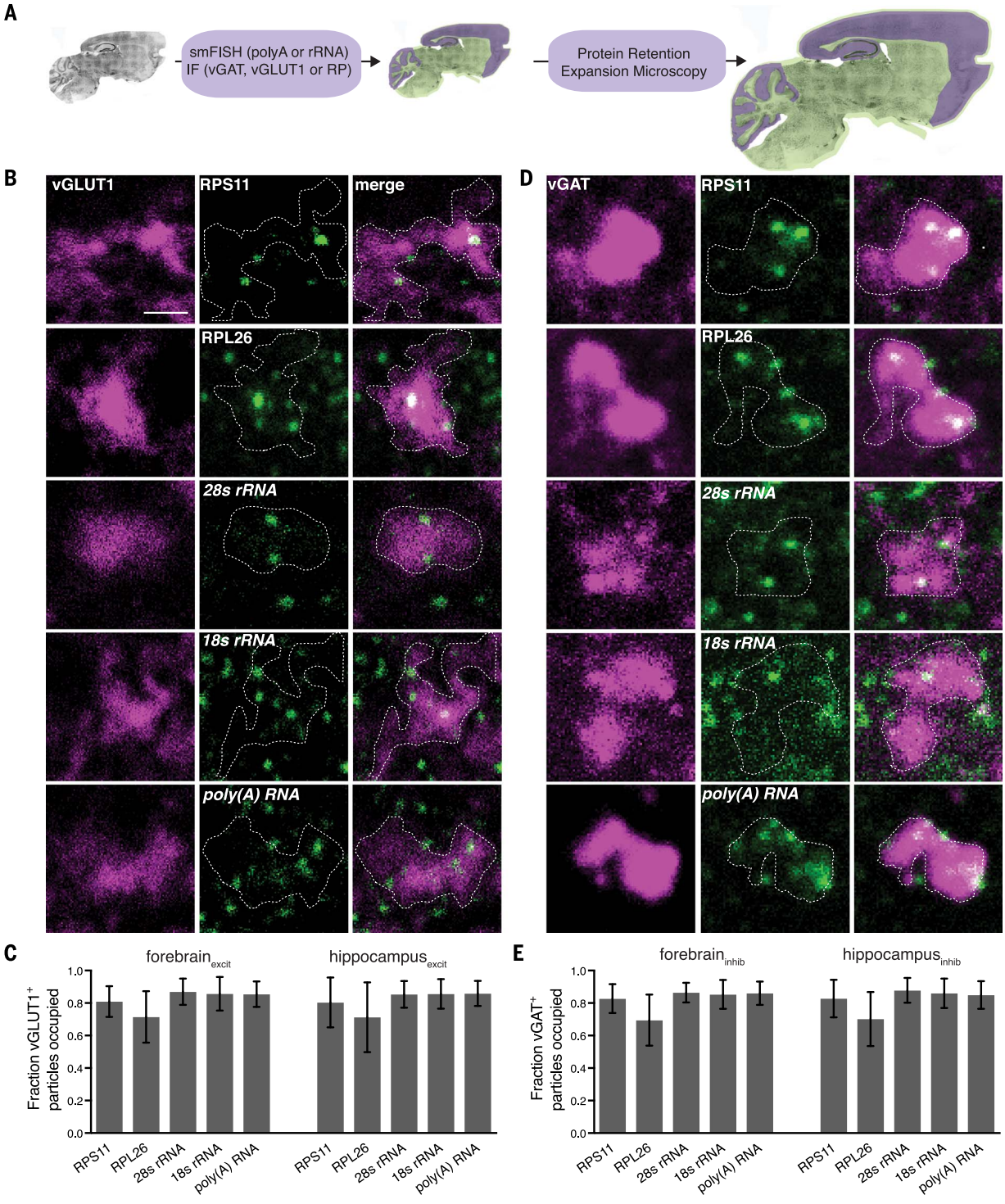

Fig. 1. Abundant ribosomes and mRNA in presynaptic compartments of the mature mouse forebrain and hippocampus. (**A**) Scheme indicating the experimental workflow. Sagittal brain slices from adult mice were processed for FISH and fluorescent immunostaining (IF) for presynaptic terminal types, excitatory (vGLUT1) or inhibitory (vGAT), and then subjected to a protein retention expansion microscopy protocol (see methods). For illustration purposes, a brain section is pseudocolored to indicate the distribution of RNA (green) and vGLUT1 (lavender). smFISH, single-molecule FISH; RP, ribosomal protein. (**B** and **D**) Representative images of expanded presynaptic compartments, chosen for their positive (B) vGLUT1$^+$ or (D) vGAT$^+$ signal (magenta), showing the presence of both small and large ribosomal proteins (green) (top two rows), large and small rRNAs (green) (third and fourth rows), or poly (A)$^+$ RNA (green) (bottom row). The merged images (the last image in each row) show both signals. Outlines indicate the area quantified. Scale bar, 1.5 um. (**C** and **E**) Bar graphs showing analysis for all vGLUT1$^+$ compartments (C) and all vGAT$^+$ terminals (E) analyzed from the forebrain and the hippocampus. More than 75% of all vGLUT1$^+$ terminals and >75% of all vGAT+ terminals contained ribosomal proteins and RNA, as well as poly (A)$^+$ RNA. Data were acquired from four different animals per condition. The mean and SEM are plotted. For additional details, see table S2. excit, excitatory; inhib, inhibitory.

Corrected 11 February 2020. See full text.

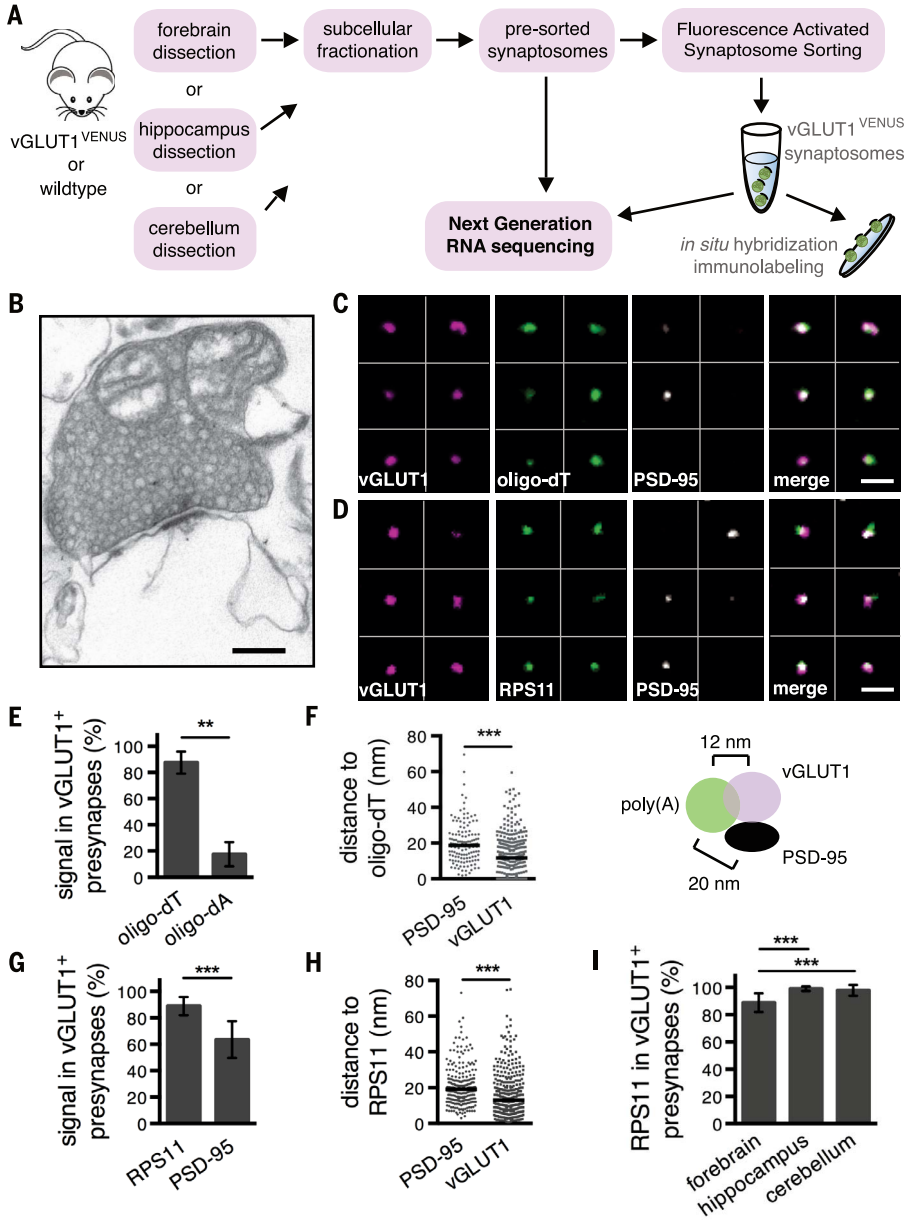

Fig. 2. Presynaptic compartments isolated from adult mouse brain contain spatially organized mRNA and ribosomes. (**A**) Scheme showing experimental flow for analysis of the global (presorted) synaptosome and fluorescently sorted vGLUT1$^+$ synaptosome populations. (**B**) Representative electron micrograph of a presorted synaptosome. Scale bar, 200 nm. (**C** and **D**) Example confocal images of sparsely plated vGLUT1$^+$ synaptosomes labeled by FISH and IF showing the vGLUT1$^+$ signal in each synaptosome panel, as well as the presence or absence of poly (A)$^+$ RNA (C) or RPS11 (D) and PSD-95 for the same samples. Merged images are shown in the last panel. See fig. S7 for images for oligo(dA). Scale bars, 5 μm. (**E**) Bar graph for all synaptosomes analyzed (the analysis includes sorted and presorted, as the two populations yield similar results) showing that 87.6 ± 8.4% of all vGLUT1$^+$ terminals were positive for a FISH oligo(dT) probe whereas <17.5 ± 9.2% were positive for a FISH oligo(dA) probe [n = 921 synaptosomes for oligo(dT) and n = 1069 synaptosomes for oligo(dA), from two biological replicates]. $^{**}P \leq 0.01$; unpaired t test. (**F**) Plot of all data points for sorted synaptosomes and the median (left) and a scheme (right) showing center-to-center distances between fluorescence signals. The center of the oligo(dT) signal (green) was on average 12.8 nm from the center of the vGLUT1 signal (lavender) and 20.0 nm from the PSD-95 signal (black) (n = 317 synaptosomes for vGLUT1 and n = 134 synaptosomes for PSD-95). $^{***}P \leq 0.001$; unpaired t test. (**G**) Bar graph for all synaptosomes analyzed (the analysis includes sorted and presorted populations) showing that 88.9 ± 6.9% of all vGLUT1$^+$ terminals were positive for RPS11 and 63.5 ± 14.0% were positive for PSD-95 (n = 568 terminals from three biological replicate experiments). $^{***}P \leq 0.001$; unpaired t test. (**H**) Plot showing the center-to-center distances between fluorescence signals. The center of the RPS11 signal was on average 19.5 nm from the PSD-95 signal and 15.9 nm from the center of the vGLUT1 signal. $^{***}P \leq 0.001$; unpaired t test. (**I**) Bar graph for all synaptosomes analyzed [forebrain data are the same as those in (F); for the hippocampus and cerebellum, we analyzed vGLUT1$^+$ sorted synaptosomes] showing that >80% of all vGLUT1$^+$ terminals were positive for RPS11 in all three brain regions (forebrain = 88.9 ± 6.9%; hippocampus = 99.1 ± 1.4%; cerebellum = 97.9 ± 4.0%) (n = 568 forebrain terminals, n = 834 hippocampus terminals, and n = 236 cerebellum terminals from at least two biological replicate experiments). $^{***}P \leq 0.001$; Kruskal-Wallis nonparametric test followed by Dunn's multiple comparison test. All data are shown as mean ± SD.

knock-in mice, in which all vGLUT1^{VENUS}-positive (vGLUT1$^+$) synapses were fluorescently labeled (*30*), we prepared and sorted vGLUT1$^+$ synaptosomes for FISH, immunocytochemistry (Fig. 2, C to I), and ultimately RNA sequencing (Fig. 3). We first examined whether the vGLUT1$^+$ sorted synaptosome population, reflecting the composition of excitatory synapses in vivo, had the molecular elements that we detected in the expanded hippocampal and forebrain tissues (Fig. 1, B and C). By using sparse plating of individual vGLUT1$^+$ synaptosomes combined with imaging, we determined the incidence of poly (A)$^+$ mRNA and ribosomal proteins, together with that of a postsynaptic density marker protein, PSD-95 (Fig. 2, C to I). More than 80% of all sorted vGLUT1$^+$ synaptosomes contained poly (A)$^+$ mRNA (Fig. 2, C and E, and fig. S7), ribosomal proteins (Fig. 2, D, G, and I), and rRNA (fig. S7). As expected, a smaller fraction (~60%) of synaptosomes were associated with PSD-95 (Fig. 2, C, D, and G). To determine whether this high translational capacity is a universal feature of excitatory synapses, we also examined ribosomal protein labeling in vGLUT1$^+$ synaptosomes sorted from the adult mouse hippocampus or cerebellum. We found a similarly high occupancy of ribosomes in the hippocampal and cerebellar excitatory synapses: ~90% were positive for ribosome immunolabeling (Fig. 2I). In addition, as observed in adult brain slices, a large majority of the vGAT$^+$ immunolabeled synaptosomes were also immunopositive for ribosomes (fig. S7).

We took advantage of the punctate nature of the imaged fluorescence signals to calculate the center-to-center distances for poly (A)$^+$ mRNA or RPS11 and vGLUT1 or PSD-95 (Fig. 2, F and H). By using stimulated emission depletion microscopy (STED), we confirmed the tight spatial relationship between vGLUT1 and RPS11 (fig. S8). The measured distances were consistent with the localization of the presynaptic translation

Corrected 11 February 2020. See full text.

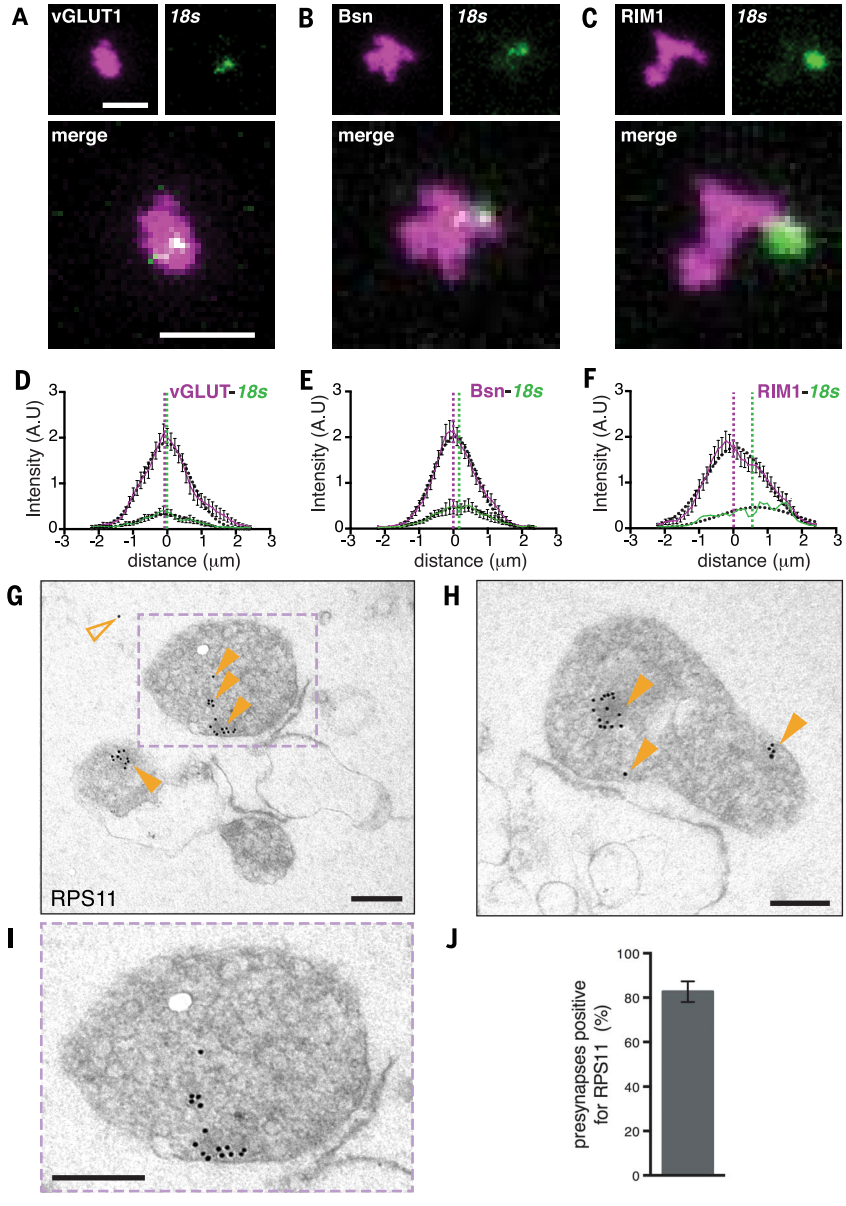

Fig. 3. Ribosomes are spatially offset from the active zone in presynaptic terminals. (**A** to **C**) Synaptosomes were immunostained for vGLUT1 (A), bassoon (B), or RIM1 (C) (magenta) and processed for FISH against 18S rRNA (green). Scale bar, 2.5 um. (**D** to **F**) A line scan analysis was performed (see methods) to assess the spatial distribution of rRNA in the synaptosomes relative to the pool of synaptic vesicles or the active zone. Graphs depict the signal distribution for either the presynaptic marker (solid magenta curve) or the rRNA (solid green curve). Dotted lines indicate the peaks of the Gaussian fits (black dotted curves), showing that the ribosomes were offset from the active zone. n = 40 synaptosomes analyzed from three biological replicates. Error bars correspond to SEM. For additional details, see table S2. A.U., arbitrary units. (**G** to **I**) Representative electron micrographs of presorted synaptosomes after postembedding immunostaining with an anti–ribosomal protein RPS11 antibody. (G) Electron micrograph showing three terminals, two of which were associated with a postsynaptic membrane and two of which contained multiple gold particles (closed arrowheads) reflecting the presence of ribosomes in these compartments. Only one gold particle (open arrowhead) is present in the field of view outside of the terminals. Scale bar, 200 nm. (H) Electron micrograph showing a terminal containing multiple gold particles (closed arrowheads) and an open postsynaptic compartment. Scale bar, 200 nm. (I) Enlarged view of the terminal in the boxed area in (G), suggesting that ribosomes are not present in the active zone. Scale bar, 200 nm. (**J**) Bar graph showing the percentage of RPS11$^+$ synapses from immuno-EM images (82.7 ± 4.7%; n = 2 biological replicates and 147 terminals counted). Data are shown as mean ± SD.

machinery as slightly offset from the synaptic cleft (Fig. 2, H and I). This suggests that presynaptic translation can occur away from the active zone. In addition, we optimized expansion microscopy for application to synaptosomes and further probed the spatial organization of the ribosome population relative to the active zone. Synaptosomes were visualized by using markers differentially localized within boutons: vGLUT1 (associated with synaptic vesicles), bassoon (a soluble scaffolding protein), and RIM1 (an active-zone membrane protein). Consistent with the above data, in the expanded synaptosomes ribosomes (measured with 18S and 28S rRNA FISH) were positioned closer to vGLUT1 and bassoon than to the active-zone membrane (measured with RIM1 immunolabeling) (Fig. 3, A to F, and fig. S8). Lastly, we used immuno–electron microscopy (EM) to detect the ribosomal protein RPS11 in the presorted synaptosome. We detected RPS11 in a majority of the presynaptic terminals (Fig. 3, G to J), and the localization, again offset from the active zone, was consistent with the above data. Thus, the majority of presynaptic terminals, both excitatory and inhibitory, contained both poly (A)$^+$ mRNA and ribosomal protein, indicating a clear capacity for protein synthesis.

The presynaptic transcriptome of vGLUT1$^+$ terminals

To discover the transcriptome present in adult mouse presynaptic boutons, we used RNA sequencing to identify the mRNA populations of both the presorted and vGLUT1$^+$ synaptosomes (see methods). From three biological replicates for each group (presorted and sorted), we obtained a total of 244 million (Mio) reads that, after genome alignment, yielded 12,730 transcripts detected in all replicates from both groups (196 Mio uniquely mapped reads in total) (Fig. 4A and table S1). We analyzed the transcripts that were significantly enriched or depleted in the vGLUT1$^+$ sorted population (relative to those in the presorted synaptosomes) and identified 468 and 792 transcripts, respectively (Fig. 4, A and B, and table S1). Enriched transcripts overlapped to varying degrees with those identified in prior synaptic sequencing studies (fig. S9). Gene Ontology (GO) analysis of the vGLUT1$^+$ enriched transcripts [using the ~12,700 transcripts from the input forebrain transcriptome (table S1) as a background comparison set] revealed a significant overrepresentation of genes coding for presynaptic active-zone proteins, ribosomal proteins, and other groups such as synapse proteins (Fig. 4C). Among the most enriched in the vGLUT1$^+$ presynaptic transcriptome were many well-known presynaptic proteins, including those encoded by *Bassoon* (*Bsn*), *Rims1* to *-3*, and *Stx6*, as well as signaling molecules, such as those encoded by *Sergef* and *Rapgef4* (Fig. 4, B and F), and mitochondrial proteins (fig. S9). Among the 792 transcripts depleted in the vGLUT1$^+$ transcriptome were many coding for neurotransmitter receptors of the GABA (γ-aminobutyric acid) and AMPA families, indicating the depletion of postsynaptic and dendritic components through

Corrected 11 February 2020. See full text.

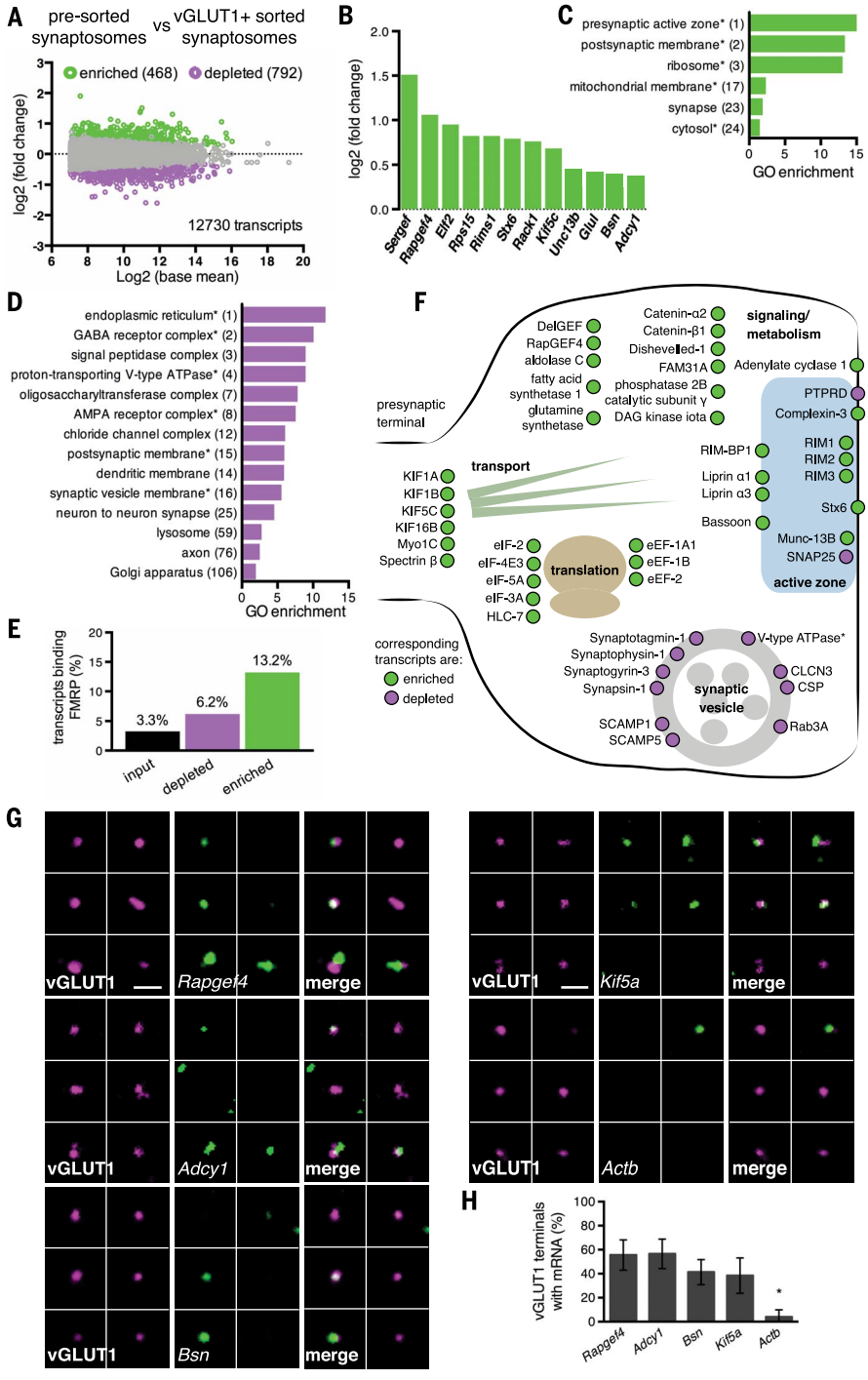

Fig. 4. An excitatory presynaptic transcriptome from mature mouse synapses. (**A**) Differential expression analysis (see methods) showing the relationship between expression (reads per million) and the significant enrichment (green dots) or depletion (magenta dots) in the vGLUT1$^+$ sorted versus presorted synaptosomes. (**B**) Selected list of significantly enriched individual vGLUT1$^+$ presynaptic transcripts. (**C**) Selected GO annotations of transcripts significantly enriched by vGLUT1$^+$ sorting. (**D**) Selected GO annotations of transcripts significantly depleted by vGLUT1$^+$ sorting. The ranking of each category is given in parentheses in (C) and (D). Asterisks indicate that the GO annotation name was shortened; complete names are available in table S1. ATPase, adenosine triphosphatase. (**E**) Comparison of the percentages of mRNAs containing FMRP binding sites in the forebrain transcriptome (input), the contaminant transcriptome (depleted), and the vGLUT1$^+$ enriched presynaptic transcriptome (enriched). (**F**) Schematic representation of a vGLUT1$^+$ presynaptic terminal with the localization of a subset of proteins encoded by mRNA detected by using next-generation RNA sequencing of synaptosomes. Many presynaptic active zone–related mRNAs are enriched by the sorting procedure (green), whereas synaptic vesicle–related mRNAs are either significantly depleted (magenta) or not enriched by sorting. Raw data and the complete GO and gene lists are available in table S1. DAG, diacylglycerol; eIF, eukaryotic initiation factor; eEF, eukaryotic elongation factor; HLC, guanine nucleotide–binding protein subunit β–like protein 12.3; PTPRD, protein tyrosine phosphatase, receptor type D. (**G**) FISH conducted on isolated vGLUT1$^+$ synaptosomes validating the presence of *Rapgef4*, *Adcy1*, *Bsn*, and *Kif5* mRNAs and the absence of *Actb* mRNA in vGLUT1$^+$ terminals. (**H**) Bar graph analysis of FISH data indicating the percentage of vGLUT1$^+$ synaptosomes that have the indicated mRNA (n = 939 synaptosomes for *Rapgef4*, n = 551 for *Adcy1*, n = 1437 for *Bsn*, n = 1292 for *Kif5*, and n = 359 for *Actb*; vGLUT1$^+$ terminals were from at least two biological replicate experiments). Data are shown as mean ± SD (*Rapgef4* = 55.6 ± 12.6%; *Adcy1* = 56.5 ± 12.3%; *Bsn* = 41.3 ± 10.4%; *Kif5a* = 38.4 ± 14.7%; and *Actb* = 4.0 ± 6.0%). *$P \leq 0.05$; Kruskal-Wallis nonparametric test followed by Dunn's multiple comparison test. All scale bars, 5 μm.

our synaptosome sorting (Fig. 4, D and F). Also, transcripts coding for membrane proteins (fig. S9), including ER proteins such as those encoded by *Ergic1*, *Calr*, or *Sec62*, were diminished in the vGLUT1$^+$ sorted synaptosomes (fig. S9 and table S1). There was also a clear depletion of transcripts coding for integral synaptic vesicle proteins (Fig. 4, D and F, and table S1), consistent with a recent report of somatic vesicle biogenesis and transport (*31*). Of note, among the 468 transcripts enriched in vGLUT1$^+$ terminals, 62 were known targets of the RNA binding fragile X mental retardation protein (FMRP), the loss of which causes fragile X syndrome (Fig. 4E and table S1) (*32*). We validated the presence (or absence) of several of the vGLUT1$^+$ enriched transcripts, including those for *Rapgef4*, *Adcy1*, *Bsn*, *Kif5a*, and *Actb*, in sparsely plated vGLUT1$^+$ synaptosomes by using FISH (Fig. 4, G and H, and fig. S10). Thus, presynaptic compartments from adult mouse forebrain contained the requisite machinery and a diverse mRNA population for protein synthesis.

Abundant protein synthesis is detected in presynaptic terminals

To obtain direct evidence for protein synthesis in synaptic compartments, particularly presynaptic boutons, we adapted the puromycin-based metabolic labeling strategy (*33*) for detection with EM or expansion microscopy. Cultured hippocampal neurons were briefly labeled with puromycin and then fixed and processed for EM by using immunogold labeling with an anti-puromycin antibody (see methods). Using transmission EM,

Corrected 11 February 2020. See full text.

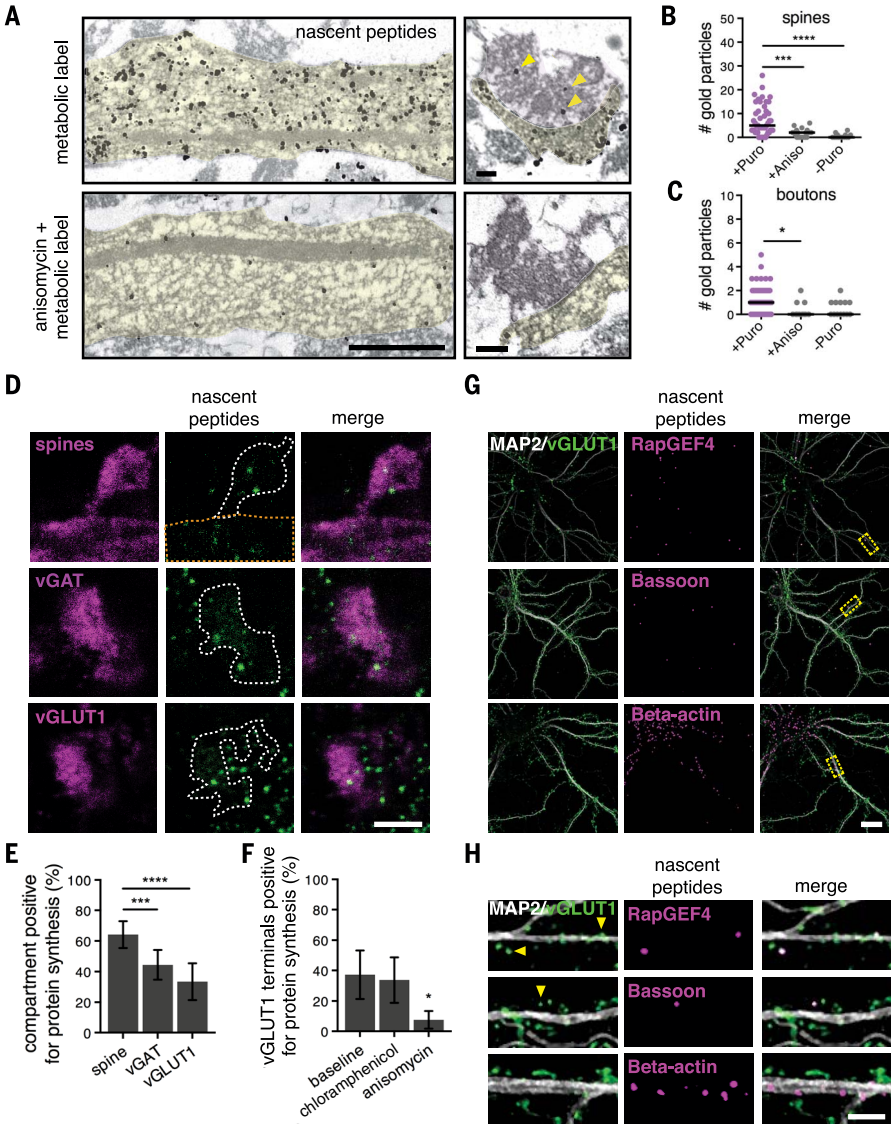

Fig. 5. Pre- and postsynaptic compartments actively translate protein in the absence of external stimulation. (**A**) Electron microscope images of cultured hippocampal neurons metabolically labeled with puromycin for 10 min and then detected by using immunogold (see methods). Electron-dense particles indicate sites of protein synthesis. Shown are dendritic segments (left) and synapses (right) with gold particles present throughout the dendrite, as well as in both the presynaptic (lavender) and postsynaptic (pale green) compartments in the absence of anisomycin. Arrowheads indicate protein synthesis sites in presynaptic boutons. Scale bars, 1 and 0.2 μm for the dendrite and synapse, respectively. (**B** and **C**) Plots indicating the numbers of gold particles and the corresponding medians reflecting nascent-protein immunogold labeling in dendritic spines [mean number in cultures with puromycin (+puro) (the metabolic label) = 5; in cultures with anisomycin (+aniso) = 2; and in cultures without puromycin (−puro) = 0] (n = 49 spines for +puro, n = 21 for +aniso, and n = 14 for −puro) (B) and presynaptic boutons (mean number of particles for +puro = 1; for aniso = 0; and for −puro = 0) (n = 54 boutons for +puro, n = 11 for +aniso, and n = 13 for −puro) (C) in the presence of puromycin (10-min incubation) with or without the translation inhibitor anisomycin (40-min incubation in total) and in the absence of puromycin. Quantifications were obtained from two biological replicates. *$P \leq 0.05$; Kruskal-Wallis nonparametric test followed by Dunn's multiple comparison test. (**D**) Representative images of expanded cultured hippocampal neurons after 5 min of metabolic labeling and immunolabeling showing nascent protein detected in dendritic spines, excitatory presynaptic boutons, or inhibitory presynaptic boutons. Dashed lines indicate the area quantified (white) and the parent dendrite (orange). (**E**) The quantification of metabolic labeling showed that a large fraction of both pre- and postsynaptic compartments were translationally active within 5 min of metabolic labeling. Data are shown as mean ± SD (fraction of compartment positive for protein synthesis: spines = 64.2 ± 8.8%; vGAT compartment = 44.4 ± 9.7%; vGLUT1 compartment = 37.5 ± 12.0%). ***$P \leq 0.001$; ****$P \leq 0.0001$; Kruskal-Wallis nonparametric test followed by Dunn's multiple comparison test. (**F**) The quantification of puromycin occupancy revealed that the inhibition of mitochondrial protein synthesis had no effect in vGLUT1$^+$ puncta. Representative images are shown in fig. S12. Data are shown as mean ± SD (vGLUT1 terminals positive for protein synthesis: baseline = 37.3 ± 15.9%; samples with chloramphenicol = 33.7 ± 15.0%; samples with anisomycin = 7.6 ± 5.8%). n = 3 biological replicates, with 300 vGLUT1$^+$ terminals quantified. *$P \leq 0.05$; Dunnett's multiple comparison test. (**G** and **H**) Representative images showing newly synthesized proteins of interest, RapGEF4 and bassoon, which were also identified as transcripts enriched in the vGLUT1$^+$ transcriptome (Fig. 4, B, F, and G). Boxed areas in (G) are magnified in (H), and arrowheads point to presynaptic terminals positive for newly synthesized proteins of interest. Scale bars, 20 μm for (G) and 5 μm for (D) and (H).

we were able to identify, on the basis of morphological features (see methods), both dendrites and synapses, including presynaptic boutons, in the images (Fig. 5A). A high fraction of presynaptic boutons and postsynaptic spines contained puromycin-positive gold particles, indicating active protein synthesis within the last 10 min (Fig. 5, A to C). The inclusion of the protein synthesis inhibitor anisomycin or the omission of puromycin led to a marked reduction in the number of gold particles detected (Fig. 5, A to C, and fig. S11).

The thin nature of the EM sections precludes a three-dimensional (3D) analysis and could result in an underestimation of ongoing protein synthesis in pre- and postsynaptic compartments. Thus, to address the frequency of translation in a well-resolved 3D volume of both presynaptic boutons and dendritic spines, we used metabolic labeling in expanded cultured hippocampal neurons (Fig. 5D). Together with 5 min of metabolic labeling of nascent protein synthesis, we conducted immunocytochemical analyses using presynaptic labeling (with vGLUT1 or vGAT for excitatory or inhibitory terminals) and postsynaptic labeling (with mCherry volume fill). By analyzing the coincidence of the synaptic markers with the metabolic label (again, resolved in individual z sections), we discovered that an average of ~37 and 61% of excitatory pre- and postsynaptic compartments, respectively, and ~44% of inhibitory presynaptic terminals underwent active translation. The protein synthesis signal was markedly reduced by the addition of the protein synthesis inhibitor anisomycin (fig. S12). Because mitochondria occupy ~48% of all presynaptic terminals (*34*), we asked whether any of the presynaptic metabolic label corresponded to mitochondrial protein synthesis. The positive metabolic label in presynaptic terminals (which overlaps with either vGLUT1 or vGAT compartments) was resistant to chloramphenicol (an

Corrected 11 February 2020. See full text.

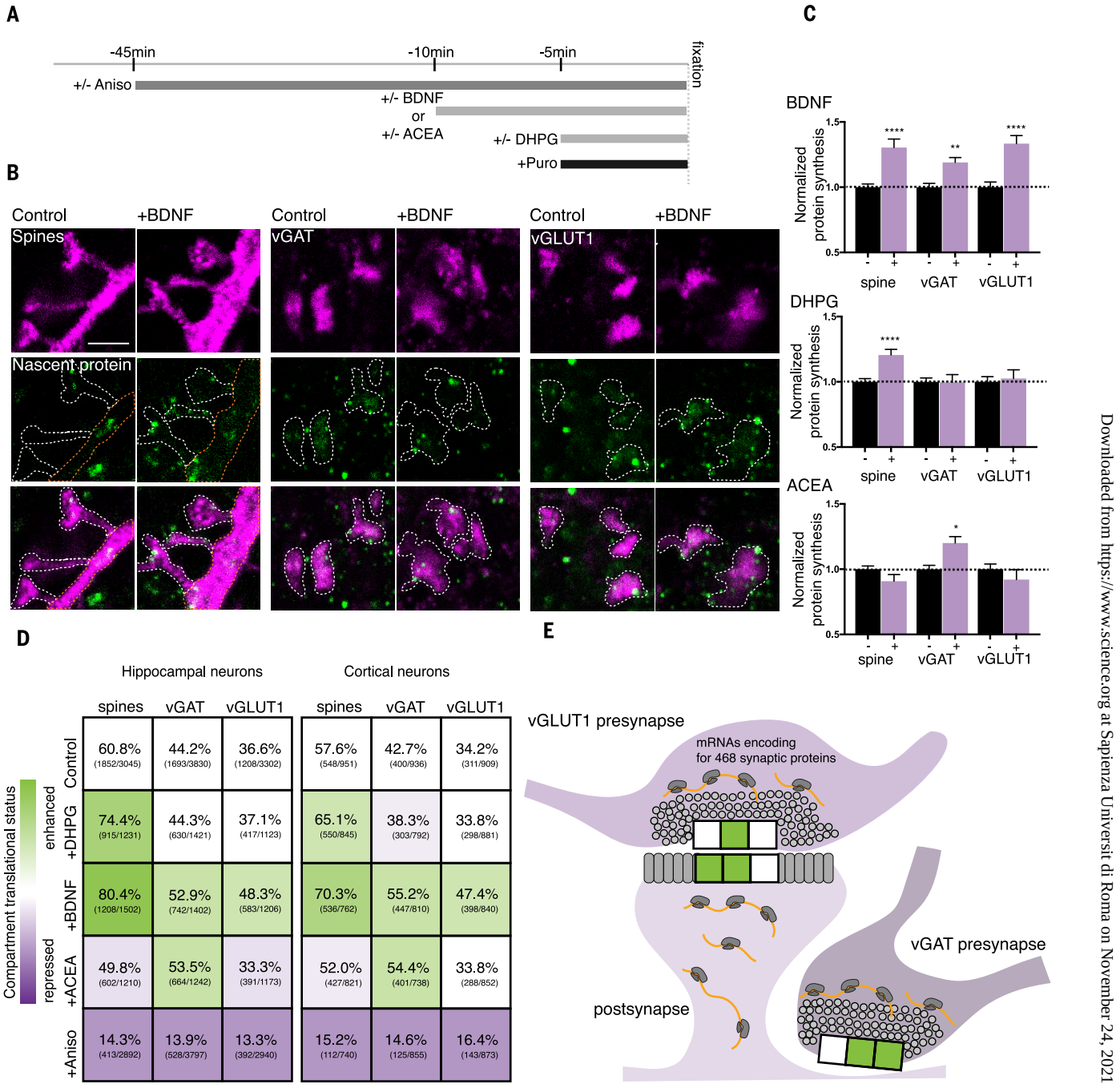

Fig. 6. Compartment-specific translation patterns decode different forms of plasticity. (**A**) Scheme showing the timing of the different plasticity induction protocols and the metabolic labeling (+puro). (**B**) Representative images from hippocampal cultures showing both the immunostained and metabolically labeled compartments, indicating newly synthesized protein following expansion microscopy for one of the plasticity conditions (±BDNF). Outlines indicate the area quantified (white) and the parent dendrite (orange). Scale bar, 5 μm. (**C**) Bar graphs indicating the specific translation pattern in different subcellular compartments (vGAT$^+$ or vGLUT1$^+$ presynaptic terminals or spines) after the three different plasticity treatments, normalized to the control condition in hippocampal cultures (n = 4 to 6 biological replicates per condition). For total puncta counted, see the numbers in the matrix shown in (D). *$P \leq 0.05$; **$P \leq 0.01$; ****$P \leq 0.0001$; unpaired t tests. For all conditions, see fig. S13. (**D**) Matrices for hippocampal and cortical neurons showing both the synaptic compartment (spine, excitatory presynaptic compartment, or inhibitory presynaptic compartment) and the plasticity agonist (BDNF, DHPG, or ACEA) applied and the percentage of compartments that exhibited protein synthesis. Shown in parentheses are the numbers of labeled compartments over the total number of compartments examined. Colors represent the change in protein synthesis, with green and lavender indicating the stimulation or repression of protein synthesis, respectively (see the color bar). (**E**) Summary scheme indicating how each different form of plasticity examined has a specific translational signature. The three compartments represented by the horizontal boxes indicate the stimulation of protein synthesis by DHPG, BDNF, or ACEA, in that order.

inhibitor of prokaryotic and mitochondrial protein synthesis) (Fig. 5F and fig. S12). Consistent with this, mitochondria immunodetected with anti-TOMM20 antibody did not overlap with either the vGLUT1 or vGAT immunolabeled compartments (fig. S12).

We next validated the local translation of some specific candidate mRNAs, identified in the presynaptic transcriptome (Fig. 4), by using puromycylation with a proximity ligation assay (Puro-PLA) (*35*) together with immunolabeling to identify postsynaptic and presynaptic compartments (with anti-MAP2 and vGLUT1 antibodies, respectively). With just 5 min of metabolic labeling, we visualized the synthesis of both RapGEF4 and bassoon in presynaptic compartments (Fig. 5, G and H, fig. S11). Thus, excitatory and inhibitory presynaptic boutons (as well as postsynaptic spines) exhibited local translation with a high frequency in the absence of any exogenous stimulation.

Differential compartment-specific regulation of protein synthesis by plasticity

Local translation is required for several forms of synaptic plasticity, including, but not limited to, potentiation induced by neurotrophins (*36*) and depression induced by the activation of metabotropic glutamate receptor 1 or 5 ($mGluR_{1/5}$) (*37*) or by endocannabinoids (*16*). Capitalizing on our ability to visualize the protein synthesis that occurs in three different synaptic compartments (the dendritic spine and both excitatory and inhibitory presynaptic boutons), we examined the translational signature of these three different forms of plasticity. We treated cultured hippocampal or cortical neurons with brain-derived neurotrophic factor (BDNF), an $mGluR_{1/5}$ agonist [(*S*)-3,5-dihydroxyphenylglycine hydrate (DHPG)], or an endocannabinoid CB1 receptor agonist [arachidonyl-2-chloroethylamide (ACEA)], adding a metabolic label for the last 5 min of each treatment (Fig. 6A). Immunocytochemical detection of nascent protein and markers of each synaptic compartment was conducted, and the samples were then subjected to expansion microscopy. The pattern of protein synthesis in the three compartments of interest, in both brain areas, indicated that each type of plasticity yielded a distinct constellation of synaptic translation loci: BDNF caused an increase in local translation in dendritic spines and both excitatory and inhibitory boutons (Fig. 6, B to E), DHPG caused an increase in dendritic spines only, and ACEA caused an increase in inhibitory boutons exclusively (Fig. 6, C to E). The addition of anisomycin significantly reduced the signal in all conditions (fig. S13). This pattern, although clearly evident in the synaptic compartments, was not observed in either the soma or the total dendrite, strongly suggesting a synaptic, localized response (fig. S13). In separate experiments, we examined whether the three above-mentioned agonists changed the occupancy of poly $(A)^+$ mRNA, and we found no significant change (fig. S13). Thus, the compartment-specific translation observed as described above was mediated by local, enhanced translation of mRNAs already resident at the synapse. Furthermore, our results provide subcellular resolution on the local proteomic remodeling that drives different forms of synaptic plasticity.

Discussion

In this study, we investigated the localization and stimulation of protein synthesis in mature synapses and unambiguously identified protein synthesis machinery and translation in individual presynaptic compartments from three different brain areas. In adult rodent brain slices and cultured hippocampal neurons, we found that >75% of both excitatory and inhibitory presynaptic terminals [see also (*16*)] contained rRNA, ribosomes, and poly $(A)^+$ mRNA. Both light (confocal and super-resolution) microscopy and EM revealed that, in the absence of overt stimulation, there was a surprisingly high level of ongoing protein synthesis in both pre- and postsynaptic compartments: Within only 5 min of labeling, ~40% of both excitatory and inhibitory presynaptic terminals and ~60% of dendritic spines exhibited active translation. Puromycin, a tRNA mimic, was used to metabolically label nascent proteins (*33*); we used an optimized low concentration to label nascent peptides while avoiding a complete block of protein synthesis. The stringency of our presynaptic translation measurements (e.g., the requirement that the metabolic labeling spatially overlap with vesicular marker immunolabeling) may also lead to an underestimate of actively translating compartments, particularly when the measurements are compared with the spine measurements where a volume-filling label was used. We therefore believe that the above values likely represent a conservative estimate of the fraction of compartments undergoing translation in the labeling window. Our plasticity data confirm that we have identified a "lower bound": Even higher fractions of actively translating compartments (~81, 54, and 48% of spines and vGAT and vGLUT1 terminals) were observed after 5 min of metabolic labeling.

Thousands of mRNA transcripts are present distally in neuronal processes, where they can be locally used for protein synthesis (*38*–*41*). Notably, the transcriptome of retinal ganglion cell axons has been characterized during development (*42*, *43*), and the retinal ganglion cell translatome has been identified in the adult mouse (*15*). In this study, by using mature mouse forebrain synaptosomes that are enriched for $vGLUT1^+$ presynaptic terminals, we identified ~450 transcripts that were enriched, relative to the "presorted" or bulk synaptosome transcriptome. There were also many transcripts shared between the presorted and sorted synaptosomes (Fig. 4A and table S1) that were not enriched in the $vGLUT1^+$ transcriptome but likely represent important translation targets within post- and/or presynaptic compartments. Within this $vGLUT1^+$ enriched transcriptome, we detected many mRNAs that code for proteins that regulate vesicle release probability, including those encoded by *Rim* genes, *Adcy1*, and *Bsn*. By using Puro-PLA (*35*), we validated the synthesis of several presynaptic proteins, including RapGEF4 and bassoon, in identified nerve terminals within minutes of metabolic labeling. Some of the earliest studies suggesting translation in axons observed radioactive labeling in synaptosomes (*44*, *45*). Notably, mRNAs coding for synaptic vesicle proteins were lacking in our $vGLUT1^+$ transcriptome. Perhaps local translation of presynaptic proteins could work in concert with the well-documented transport of presynaptic proteins and complexes within axons (*46*) to supply and regulate neurotransmitter release and homeostasis in mature, healthy nerve terminals.

We detected an enrichment of transcripts in several functional categories. For example, we noted an abundance of mRNAs coding for proteins that directly regulate translation, including eukaryotic initiation and elongation factors [see also (*15*)]. Although many of these proteins have been detected within dendrites (*47*, *48*), whether they are present in excess or limited quantities is unknown. Signaling events at the synapse could thus boost translational capacity by synthesizing these potentially rate-limiting regulatory elements. Local protein synthesis is dysregulated in many neurodevelopmental disorders (*49*), and recent attention has focused on a presynaptic locus of some important proteins, such as FMRP (*50*). In this regard, we note that >10% of the $vGLUT1^+$ enriched presynaptic transcripts have an FMRP-binding site (*32*). Shigeoka *et al.* also observed an abundance of FMRP targets in the retinal ganglion cell axonal translatome (*15*).

Multiple forms of synaptic plasticity involve local translation in dendrites, including BDNF-induced synaptic potentiation (*36*), mGluR-dependent long-term depression (*51*), dopamine-induced plasticity (*52*), and homeostatic plasticity (*48*), and the activation of presynaptic CB1 receptors by retrograde endocannabinoid signaling stimulates local protein synthesis in inhibitory terminals to produce long-term depression of inhibitory transmission (*16*). We found local translation in both the pre- and postsynaptic compartments to be differentially regulated by three of the above-mentioned forms of plasticity in a compartment-specific manner. These data indicate that there is also information about the recent synaptic history and the expression of plasticity in the particular pattern of translation loci in synaptic compartments. With the selection of particular mRNAs for translation on the basis of specific regulatory elements present in the 3′ untranslated regions (*53*), a distinct and remodeled synaptic proteome for each kind of plasticity can be achieved. Our findings demonstrate that local protein synthesis is a ubiquitous feature of both sides of the synapse—it occurs in both excitatory and inhibitory presynaptic boutons, as well as dendritic spines, under basal conditions and is differentially recruited in these compartments to modify local proteomes. Taken together with the well-documented system of microtubule-based transport (in both axons and dendrites) to supply both mRNA and protein, local synthesis adds an important source of protein that presumably can be exploited to alter the local proteome with spatial and temporal precision.

Corrected 11 February 2020. See full text.

Materials and methods

Cultured neurons

Dissociated rat hippocampal or cortical neuron cultures were prepared and maintained as described previously (*54*). Briefly, we dissected hippocampi or cortices from postnatal day 0 to 1 rat pups of either sex (Sprague-Dawley strain; Charles River Laboratories), dissociated the samples with papain (Sigma), and plated them at a density of 40 × 10^3 cells/cm^2 on poly-D-lysine–coated glass-bottom petri dishes (MatTek). Neurons were maintained and matured in a humidified atmosphere at 37°C and 5% CO_2 in growth medium [Neurobasal-A supplemented with B27 and GlutaMAX-I (Life Technologies)] for 18 to 21 DIV to ensure synapse maturation. All experiments complied with national animal care guidelines and the guidelines issued by the Max Planck Society and were approved by local authorities. For transfection, 7- to 11-DIV neurons were transfected with mCherry-C1 or enhanced green fluorescent protein (EGFP)–C1 by using Effectene (Qiagen) as previously described (*55*). Transfected cells were maintained for 18 to 21 DIV for experiments.

Preparation of mouse brain sections

Twelve-week-old mice were perfused with 1× phosphate-buffered saline (PBS) and 4% (v/v) paraformaldehyde (PFA) solution in PBS. Brains were dissected and sliced to 2 mm, and slices were fixed for 3 hours at room temperature. Slices were cryoprotected in 20% (w/v) sucrose in PBS (diethyl pyrocarbonate treated) overnight at 4°C and cryosectioned at a thickness of 20 μm. Samples were then stored at −20°C in 80% ethanol until use.

In situ hybridization in synaptosomes and cultured neurons

All steps were performed at room temperature, unless stated otherwise. Glass-bottom dishes with attached neurons (>21 DIV) or presorted or $vGLUT1^+$ sorted synaptosomes plated on gelatinized coverslips were fixed in 4% PFA in lysine phosphate buffer (pH 7.4) containing 2.5% sucrose for 15 to 20 min. Target-specific in situ hybridization was performed by using Stellaris probes (LGC Bioresearch) as previously described (*56*) and oligo(dT) and oligo(dA) as described in (*57*). After fixation, cells were washed in PBS plus 5 mM $MgCl_2$ and then dehydrated in 80% ethanol overnight at −20°C. Samples were rehydrated in PBS with $MgCl_2$ and subjected to two washes with 1× saline sodium citrate (SSC), followed by a 5-min wash in 2× SSC plus 30% formamide for 5 min. Biotin-labeled probes for 18S and 28S rRNAs (Stellaris, Biosearch Technology) and 18-nucleotide oligo(dT) and oligo(dA) oligomers (Eurofins) were diluted into 100 μl of hybridization buffer and incubated on cells overnight at 37°C. After probe hybridization, samples were washed twice in 2× SSC plus 30% formamide for 30 min each time and then washed five times in 1× SSC. After the completion of in situ hybridization, samples were washed with PBS and subsequently processed for immunofluorescence (IF). For RNase A/T1 controls, 1 ml of digestion buffer (10 mM tris-HCl, 300 mM NaCl, 5 mM EDTA) was added to samples with and without 20 μl of RNase A/T1 (Thermo Fisher) for 30 min at 37°C after sample rehydration. For permeabilization controls, ethanol dehydration series were omitted.

In situ hybridization in tissue

After rehydration, samples were postfixed for 5 min in ice-cold 4% PFA and then washed in 2× SSC. Samples were treated with 0.1 M triethanolamine-HCl (pH 8.0) with acetic anhydride for 10 min to reduce nonspecific hybridization. After being washed in ice-cold H_2O, samples were incubated in ice-cold methanol-acetone and then washed in ice-cold 1× SSC. Samples were blocked for endogenous biotin by using streptavidin for 30 min at 37°C followed by a biotin wash (Thermo Fisher) for 5 min. Samples were then incubated in 2× SSC for 10 min and next in 2× SSC plus 50% formamide for 1 hour. FISH probes were diluted to 2× in 200 μl of hybridization buffer and incubated overnight at 37°C. Samples were washed five times in 2× SSC plus 50% formamide for 60 min each time at 37°C and then five times in 2× SSC for 10 min each time. After the completion of in situ hybridization, samples were washed with PBS and subsequently processed for IF.

IF in synaptosomes and cultured neurons

All steps were performed at room temperature, unless stated otherwise. Glass-bottom dishes with attached neurons (18 to 21 DIV) or presorted or $vGLUT1^+$ sorted synaptosomes plated on gelatinized coverslips were fixed in 4% PFA in lysine phosphate buffer (pH 7.4) containing 2.5% sucrose for 15 to 20 min. Cells were then permeabilized for 10 min in PBS plus 0.5% Triton-X 100 (Sigma). Samples were incubated in blocking buffer (4% goat serum in PBS) or biotin-free blocking buffer [4% biotin-free bovine serum albumin (BSA) in PBS for FISH experiments] for 30 min. After three washes in PBS for 5 min each, samples were incubated in blocking buffer (4% goat serum in PBS for cell culture experiments or 4% biotin-free BSA in PBS for cell culture FISH experiments) for 1 to 2 hours with secondary antibodies. We used the following antibodies: guinea pig anti-MAP2 (Synaptic Systems, 1:2000), rabbit anti-biotin (Bethyl, 1:1000), rabbit anti-biotin (Cell Signaling, 1:1000), chicken anti–green fluorescent protein (GFP) (Aves, 1:1000), chicken anti-mCherry (Abcam, 1:1000), mouse anti–PSD-95 (Thermo Fisher Scientifics, 1:1000), mouse anti-synaptopodin (Merck, 1:500), rabbit anti-calreticulin (Abcam, 1:1000), guinea pig anti-Homer1 (Synaptic Systems, 1:1000), mouse anti-puromycin (Kerafast, 1:500 to 1:1000), guinea pig anti-vGLUT1 (Synaptic Systems, 1:500 to 1:2000), guinea pig anti-vGAT (Synaptic Systems, 1:500 to 1:2000), rabbit anti-vGAT (Synaptic Systems, 1:1000), mouse anti–Smi-312 (Covance, 1:2000), rabbit anti-RPS11 (Bethyl, 1:200), and rabbit anti-RPL26 (Sigma, 1:500 to 1:1000). After three washes in PBS for 5 min each, samples were incubated in blocking buffer (4% goat serum in PBS) for 1 to 3 hours at room temperature with secondary antibodies. For expansion microscopy, we used the following dyes coupled to our secondary antibodies: Alexa 488, Alexa 568, and Abberior STAR-635.

IF in tissue sections

Brain sections were incubated in 4% goat serum with 0.5% Triton-X 100 for normal IF or in 4% biotin-free BSA with 0.5% Triton-X 100 for FISH experiments at room temperature for 4 hours. Primary antibody staining was carried out overnight in the same buffer at 4°C. Samples were washed five times in PBS before secondary antibody staining was carried out for 3 hours at room temperature.

Total protein labeling

Before permeabilization, cells or tissues were incubated with 0.2 M bicarbonate buffer supplemented with Alexa 568 NHS ester (0.5 mg/ml; Thermo Fisher) for 15 min at room temperature to label all amine groups in the sample with the Alexa dye. Samples were washed five times with PBS and used for subsequent IF or FISH experiments.

Cell treatments

For puromycin labeling experiments, cultured neurons were treated with 10 μM puromycin for 5 min, if not stated otherwise. Treatment with anisomycin (40 μM) was performed 20 to 45 min before puromycin labeling. BDNF (50 ng/ml) was added for 10 min, ACEA (50 μM) was added for 10 min, and DHPG (50 μM) was added for 5 min. For mitochondrial protein synthesis inhibition experiments, 40 μM chloramphenicol was added for 40 min before the addition of puromycin.

Expansion microscopy

After IF labeling, samples were treated with Acryloyl-X SE [6-((acryloyl)amino)hexanoic acid, succinimidyl ester] (Thermo Fisher) overnight at room temperature. After the washing steps, 200 μl of monomer solution was added to the coverslip and gelation was carried out at 37°C for 1 hour. For tissue sections, water was replaced with 4-hydroxy–TEMPO (2,2,6,6-tetramethylpiperidin-1-oxyl) (Thermo Fisher) as previously described (*22*). Tissue sections were pre-incubated in monomer solution at 4°C for 30 min before the samples were transferred to 37°C for 2 hours to allow gelation to occur. After proteinase K (NEB) digestion overnight, slightly expanded gels were transferred to a larger dish and water exchange was performed until gels were fully expanded. Expanded gels were transferred into 50-mm by 7-mm glass-bottom dishes (WillCo Wells) for imaging. Expanded gels were imaged by using Zeiss LSM780/880 confocal microscopes and a 63× oil objective (NA 1.4; PSF: LSM780, 0.240/0.258/0.729 μm; LSM880, 0.252/0.203/0.563 μm $x/y/z$) for cultured cells and synaptosomes and a 40× oil objective (NA 1.3; PSF: LSM780, 0.217/0.260/0.566 μm; LSM880, 0.238/0.253/0.636 μm $x/y/z$) for brain sections. z stacks (0.37 μm for the 63× objective

or 0.43 μm for the 40× objective) spanning the entire volume of imaged neurons, synaptosomes, or tissues were obtained and analyzed by using Imaris (Bitplane) and ImageJ.

Image analysis

To assess signal occupancy in spines or boutons, the compartment was considered positive for either puromycin or RNA if a signal was detected in at least three individual consecutive *z* slices. Presynaptic terminals were defined by vGLUT1 and vGAT signals, and spines were defined on the basis of morphology from mCherry or GFP volume filling. To be considered a spine, the compartment must be a clearly defined protrusion from the dendrite, extending at least 1 um away (in the expanded images) from the dendritic shaft. For tissue sections, because of the increased density and complexity of the samples, images were first processed in Imaris. 3D surface masks corresponding to either the vGLUT1 or vGAT signal were generated. These presynaptic surface masks were used to generate a new channel corresponding to the puromycin or RNA signal found within the 3D presynaptic volume. These images were then compressed into max intensity projections, and the number of positive vGLUT or vGAT terminals was scored, as positive or negative, on the basis of the presynaptic puromycin or RNA channel. To assess the amount of signal falling within and outside of cells, samples with total protein labeled (with Alexa 568 NHS ester) (see Total protein labeling) and FISH were analyzed in Imaris. The total protein Alexa 568 channel was used to make a 3D surface mask, and all RNA FISH signal falling within this mask was copied into a new third channel. The total signal intensity of the original RNA FISH signal channel, as well as the signal corresponding to the FISH signal within cells, was then measured. The ratio of the cellular signal to the total signal was used to assess the fraction of the signal falling within cells. For relative puromycin incorporation measurements for somata and dendrites, sum intensity projections were made by using the mCherry signal as a mask. The soma or dendrite (starting 15 μm away from the cell body and extending for at least 70 μm) was selected, and the total puromycin signal was assessed and normalized to the dendritic or soma area.

PLA

The detection of newly synthesized proteins by proximity ligation was carried out by using anti-puromycin antibodies (mouse anti-puromycin from Kerafast, 1:500 to 1:1000) in combination with protein-specific antibodies (rabbit anti-RapGEF4 from Invitrogen, 1:250; rabbit anti-bassoon from Enzo, 1:500; and rabbit anti–β-actin from Abcam, 1:1000). We used Duolink reagents (Sigma) and followed the protocol provided by the manufacturer with some modifications as described below. We routinely used rabbit PLA^{plus} and mouse PLA^{minus} probes as secondary antibodies and the Duolink detection reagent Red (Sigma) for ligation, amplification, and label probe binding. Briefly, after 5 min of metabolic labeling, hippocampal cultured neurons (21 DIV) were fixed in PBS-sucrose, permeabilized in PBS with 0.5% Triton-X 100, and blocked in PBS with 4% goat serum as described previously for immunocytochemistry assays. Next, neurons were incubated overnight at 4°C in PBS with 4% goat serum containing primary antibodies: mouse anti-puromycin, rabbit antibody to the protein of interest (anti-RapGEF4, anti-bassoon, or anti–β-actin), chicken anti-MAP2 (Abcam, 1:2000), and guinea pig anti-vGLUT1 (Synaptic Systems, 1:1000). After washing, PLA probes were applied in a 1:10 dilution in PBS with 4% goat serum for 1 hour at 37°C, washed several times with wash buffer A (0.01 M tris, 0.15 M NaCl, 0.05% Tween 20), and incubated for 30 min with the ligation reaction mixture containing the circularization oligonucleotides and T4 ligase prepared according to the manufacturer's recommendations in a prewarmed humidified chamber at 37°C. Amplification and label probe binding were performed after further washes with wash buffer A, with the amplification reaction mixture containing Phi29 polymerase and the fluorophore-labeled detection oligonucleotide prepared according to the manufacturer's recommendations in a prewarmed humidified chamber at 37°C for 100 min. Amplification was stopped by three washes in wash buffer B (0.2 M Tris, 0.1 M NaCl, pH 7.5). For better signal stability, cells were kept in wash buffer B at 4°C until imaging.

Pre-embedding immunodetection of newly synthesized proteins visualized by EM

For the detection of newly synthesized proteins in neurons, we performed pre-embedding immunodetection of puromycin as described below. All steps were performed at room temperature, if not stated otherwise. Glass-bottom dishes with attached neurons (28 DIV) were fixed in 4% PFA and 0.05% glutaraldehyde in 0.2 mM HEPES buffer (pH 7.2) for 45 min. Cells were then permeabilized for 10 min in PBS containing 0.5% Triton-X 100 (Sigma). Fixation reagents were quenched by using freshly made borohydride (1 mg/ml) in 0.2 mM HEPES (pH 8) for 10 min. Antibodies were applied on the samples in blocking buffer (PBS with 2% biotin-free BSA). After 30 min in blocking buffer, cells were incubated with mouse anti-puromycin (Kerafast, 1:2000) for 1 hour at room temperature. Before the 1-hour incubation at room temperature with anti–mouse antibody coupled to biotin (Abcam, 1:1000), we performed an endogenous biotin block (Thermo Fisher). Biotin was detected with a rabbit anti-biotin antibody coupled to 1-nm nanogold particles (1:100, FluoroNanogold Alexa 594, Nanoprobes). Samples were postfixed in 1% glutaraldehyde in 0.2 mM HEPES (pH 7.2) for 30 min, and fixation was quenched with 100 mM glycine in PBS for 10 min. Samples were then washed in water three times and then three times with 20 mM sodium citrate buffer (pH 7.0). Nanogold particles were subsequently amplified by using silver amplification for 6 min (Serva) and fixed again in 0.2% OsO_4 for 30 min. Samples were then stained with 0.25% uranyl acetate (Serva) in the dark for 30 min. After washing and dehydration with ethanol, samples were embedded in Epon (Serva). Sections (60 nm thick) were mounted onto Formvar-coated copper grids (Serva). Grids were imaged with a LEO (Zeiss) 912 OMEGA transmission electron microscope.

Synaptosome isolation

Synaptosomes were generated from forebrains, hippocampi, or cerebella of 6- to 8-week-old wild-type and $vGLUT1^{VENUS}$ knock-in mice as described previously (*27*, *28*, *30*). Our synaptosome preparation was chosen and adapted from our previously published protocol (*27*–*29*) to favor the isolation of synaptosomes with presynaptic compartments with closed membrane bilayers and postsynaptic compartments with open membrane bilayers. Briefly, the cerebellum, the forebrain, or both hippocampi from a single mouse were homogenized in 2 ml of ice-cold homogenization buffer [0.32 M sucrose, 4 mM HEPES (pH 7.4), EGTA-free protease inhibitor cocktail (Calbiochem, 1:1000), and RNasin (Promega, 1:1000)] by using a 2-ml glass-Teflon homogenizer with 12 gentle strokes. The homogenizer was then rinsed with an additional 3 ml of homogenization buffer, and the combined 5 ml of homogenate was centrifuged at 1000 × *g* for 8 min at 4°C. The supernatant was centrifuged again at 12,500 × *g* for 15 min at 4°C. The synaptosome-enriched pellet was then resuspended in 1 ml of homogenization buffer. This fraction was finally layered on top of a two-step sucrose density gradient (5 ml of 1.2 M sucrose and 5 ml of 0.8 M sucrose, 4 mM HEPES, and EGTA-free protease inhibitor cocktail, as described above). The gradient was centrifuged at 50,000 × *g* for 70 min at 4°C. Synaptosomes were recovered through the tube wall, at the interface of 0.8 and 1.2 M sucrose, by using a syringe to minimize contamination with lighter fractions enriched in myelin. The resulting fraction is referred to as presorted (sucrose) synaptosomes (or S-synaptosomes) as opposed to $vGLUT1^{+}$ sorted synaptosomes (or FASS-synaptosomes).

Postembedding immunodetection of ribosomal protein RPS11 visualized by EM

Presorted synaptosomes (~750 μl) on ice were mixed with ice-cold PBS containing EGTA-free protease inhibitor cocktail (Calbiochem, 1:1000) and RNasin (Promega, 1:1000) to obtain a final volume of 1.5 ml. Presorted synaptomes were centrifuged at 16.8 × *g* for 5 min at 4°C. All the subsequent steps were performed at room temperature unless stated otherwise. The resulting pellet was then fixed in PBS with 4% PFA and 2% glutaraldehyde for 1 hour. The pellet was then cut into two to four pieces that were washed four times in PBS and five times in H_2O before postfixation in 0.2% OsO_4 in water for 30 min. Samples were then stained with 0.25% uranyl acetate (Serva) in the dark for 30 min. After washing and dehydration with ethanol, samples

were embedded in Epon (Serva). Sections (60 nm thick) were mounted onto nickel grids (Serva) and processed for immunostaining. After three washes in tris-buffered saline with Tween 20 (TBST), grids were blocked for 10 min in TBST with 10% normal goat serum. Antibodies were applied in TBST with 1% normal goat serum. Grids were incubated with anti-RPS11 (Bethyl, 1:200) overnight in the dark. The next day, grids were washed with tris-buffered saline (TBS) five times for 3 min each time before being incubated with anti–rabbit antibody coupled to ~10-nm colloidal gold (BBI solution, 1:50) for 2 hours. Finally, grids were washed three times in TBS for 5 min each, three times in PBS for 5 min each, and three times in H_2O for 5 min each; further stained with 0.4% uranyl acetate (Serva); and contrasted with lead citrate (Merck). Grids were imaged with a LEO (Zeiss) 912 OMEGA transmission electron microscope. Control grids in which the primary antibody against RPS11 was omitted yielded no gold signal in presynaptic terminals.

FASS

S-synaptosome sorting was performed as described previously (*27*, *28*). The FACSAria-II (BD Biosciences) was operated using a 70-μm nozzle. Briefly, S-synaptosomes were stored on ice, diluted in PBS containing protease and RNAase inhibitor as described above, and labeled with the red (excitation/emission maxima, ~515/640 nm) lipophilic dye FM4-64 (Thermo Fisher Scientific, 1.5 μg/ml). Dilution was optimized to obtain an event rate of 20,000 to 25,000 events/s. FM4-64 was used to trigger the FACSAria detection on all biological membranes in the sample. A first gate delineated small particles ("singlets") and excluded events showing correlated high values for forward scatter and side scatter areas (aggregates and large particles). The singlets gate was subgated according to $vGLUT1^{VENUS}$ fluorescence intensity by using the 488 laser line. Thus, singlets were sorted into two fractions, the $vGLUT1^{VENUS}$-negative ($vGLUT1^{-}$) fraction and the $vGLUT1^{VENUS}$-positive ($vGLUT1^{+}$) fraction (fig. S10). These two fractions were subsequently either collected onto filters and processed for RNA next-generation sequencing or plated onto gelatinized coverslips at a density of 1 Mio particles per 12-mm coverslip by centrifugation at 6,800 × *g* for 34 min in 24-well plates and then processed for IF and/or in situ hybridization (see the protocol above).

STED

Super-resolved images of $vGLUT1^{+}$ sorted synaptosomes were obtained by using a Leica SP8 WLL2 inverted DMI6000 confocal microscope (Leica Microsystems, Mannheim, Germany) equipped with the 3D STED module. In the STED module, we used a 775-nm laser line to deplete Alexa 594 and ATTO-647N. We achieved two-color STED with a final ~40-nm resolution by using a 93× glycerol objective, NA 1.30, white light laser 2 (WLL2) with freely tunable excitation from 470 to 670 nm (1-nm steps), and a diode laser at 405 nm. The microscope was equipped with two internal photomultiplier tubes and two internal hybrid detectors.

RNA next-generation sequencing

Total RNAs were extracted by using TRIzol LS reagent (Thermo Fisher) and a Direct-zol RNA microprep kit (Zymo) for the following samples: the input (mouse forebrain) from wild-type and $VGLUT1^{VENUS}$ mice, presorted synaptosomes from wild-type and $VGLUT1^{VENUS}$ mice, and $vGLUT1^{+}$ sorted synaptosomes from $VGLUT1^{VENUS}$ mice (after filtration to remove the excess PBS). Total RNA libraries were generated by using a NEBNext rRNA depletion kit combined with a NEBNext Ultra II Direction RNA library prep kit for Illumina (New England Biolabs). We used 100 ng of starting RNA material for the input and presorted synaptosomes and 1 to 5 ng for $vGLUT1^{+}$ sorted synaptosomes, which corresponds to ~100 Mio synaptosomes collected per P3 fraction. In the final amplification step of the library preparation or in the PCR enrichment step, we used 12 cycles of amplification for the input and presorted synaptosomes and 16 cycles of amplification for the $vGLUT1^{+}$ sorted synaptosomes. Ultimately, we obtained cDNA libraries of ~250 bp, with each sample containing a specific barcode. Libraries corresponding to replicates 1 and 2 were sequenced together in the same sequencing run. The libraries corresponding to replicates 3 and 4 (used only as an input sample) were sequenced in a subsequent run. For sequencing, we used 10 ng of starting material for each library in a high-throughput Illumina flow cell with an Illumina NextSeq 550 instrument.

RNA sequencing data analysis

For detection and annotation of the sequencing reads, we used the following pipeline.

Genome alignment

The reference genome was mouse version mm10 from the University of California–Santa Cruz (UCSC) (*58*). Read alignment was conducted with the STAR aligner (*59*) (version 2.5.2) with the following parameters:

STAR–runMode alignRead–genomeDir $path_genome_index_mm10–readFilesCommand zcat–outStd Log–outSAMtype BAM SortedByCoordinate–outSAMstrandField intronMotif–outFilterIntronMotifs RemoveNoncanonical–alignSoftClipAtReferenceEnds No–outFilterScoreMinOverLread 0.25–outFilterMatchNminOverLread 0.25.

Annotation assignment

An annotation GTF file was downloaded from the UCSC Table Browser tool (*60*) with the following parameters.

Clade: Mammal, genome: Mouse, assembly: Dec. 2011 (GRCm38/mm10), group: Genes and Gene Predictions, track: NCBI RefSeq, table: RefSeq All (ncbiRefSeq), output format: GTF – gene transfer format (limited)

Gene expression was assessed by using featureCounts (*61*) with the following parameters: featureCounts -a path_genome_annotation -o counts.txt -t exon -Q 255 -T 12 $(ls /path/bams/files/*.bam).

Differential expression analysis

Differential expression analysis was performed by using DESeq2 in R (*62*), with the differential expression cutoff set at a 1.3-fold change and the false discovery rate set at $q \leq 0.1$ by using the Benjamini-Hochberg method (*63*, *64*).

Detection of poly(A) and poly(T) repeats

A fuzzy polyadenylate [poly(A)] match algorithm was adapted from Kent (*65*). The iterator will start at every position on the sequence with two consecutive adenine (A) [or thymine (T)] residues, setting the initial score to 10. Every match adds a score of 1, and a mismatch adds a score of −8. The iterator will stop incrementing when the score value drops below 0. The longest span of the iterator is kept per transcript as a measure of detected repeat sequence.

All Venn diagrams were obtained by using Venn 2.1 web tools (*66*).

REFERENCES AND NOTES

1. N. J. Bannister, A. U. Larkman, Dendritic morphology of CA1 pyramidal neurones from the rat hippocampus: II. Spine distributions. *J. Comp. Neurol.* **360**, 161–171 (1995). doi: 10.1002/cne.903600112; pmid: 7499561
2. A. R. Dörrbaum, L. Kochen, J. D. Langer, E. M. Schuman, Local and global influences on protein turnover in neurons and glia. *eLife* **7**, e34202 (2018). doi: 10.7554/eLife.34202; pmid: 29914620
3. C. T. Schanzenbächer, S. Sambandan, J. D. Langer, E. M. Schuman, Nascent proteome remodeling following homeostatic scaling at hippocampal synapses. *Neuron* **92**, 358–371 (2016). doi: 10.1016/j.neuron.2016.09.058; pmid: 27764671
4. C. Hanus, E. M. Schuman, Proteostasis in complex dendrites. *Nat. Rev. Neurosci.* **14**, 638–648 (2013). doi: 10.1038/nrn3546; pmid: 23900412
5. K. C. Martin, A. Ephrussi, mRNA localization: Gene expression in the spatial dimension. *Cell* **136**, 719–730 (2009). doi: 10.1016/j.cell.2009.01.044; pmid: 19239891
6. S. J. Van Driesche, K. C. Martin, New frontiers in RNA transport and local translation in neurons. *Dev. Neurobiol.* **78**, 331–339 (2018). doi: 10.1002/dneu.22574; pmid: 29314718
7. C. Glock, M. Heumüller, E. M. Schuman, mRNA transport & local translation in neurons. *Curr. Opin. Neurobiol.* **45**, 169–177 (2017). doi: 10.1016/j.conb.2017.05.005; pmid: 28633045
8. M. Crispino, J. T. Chun, C. Cefaliello, C. Perrone Capano, A. Giuditta, Local gene expression in nerve endings. *Dev. Neurobiol.* **74**, 279–291 (2014). doi: 10.1002/dneu.22109; pmid: 23853157
9. C. E. Holt, E. M. Schuman, The central dogma decentralized: New perspectives on RNA function and local translation in neurons. *Neuron* **80**, 648–657 (2013). doi: 10.1016/j.neuron.2013.10.036; pmid: 24183017
10. D. S. Campbell, C. E. Holt, Chemotropic responses of retinal growth cones mediated by rapid local protein synthesis and degradation. *Neuron* **32**, 1013–1026 (2001). doi: 10.1016/S0896-6273(01)00551-7; pmid: 11754834
11. C. J. Donnelly, M. Fainzilber, J. L. Twiss, Subcellular communication through RNA transport and localized protein synthesis. *Traffic* **11**, 1498–1505 (2010). doi: 10.1111/j.1600-0854.2010.01118.x; pmid: 21040295
12. K. M. Leung *et al.*, Asymmetrical beta-actin mRNA translation in growth cones mediates attractive turning to netrin-1. *Nat. Neurosci.* **9**, 1247–1256 (2006). doi: 10.1038/nn1775; pmid: 16980963
13. D. E. Willis *et al.*, Extracellular stimuli specifically regulate localized levels of individual neuronal mRNAs. *J. Cell Biol.* **178**, 965–980 (2007). doi: 10.1083/jcb.200703209; pmid: 17785519
14. A. Poulopoulos *et al.*, Subcellular transcriptomes and proteomes of developing axon projections in the cerebral cortex. *Nature* **565**, 356–360 (2019). doi: 10.1038/s41586-018-0847-y; pmid: 30626971

Corrected 11 February 2020. See full text.

15. T. Shigeoka *et al*., Dynamic axonal translation in developing and mature visual circuits. *Cell* **166**, 181–192 (2016). doi: 10.1016/j.cell.2016.05.029; pmid: 27321671
16. T. J. Younts *et al*., Presynaptic protein synthesis is required for long-term plasticity of GABA release. *Neuron* **92**, 479–492 (2016). doi: 10.1016/j.neuron.2016.09.040; pmid: 27764673
17. M. S. Scarnati, R. Kataria, M. Biswas, K. G. Paradiso, Active presynaptic ribosomes in the mammalian brain, and altered transmitter release after protein synthesis inhibition. *eLife* **7**, e36697 (2018). doi: 10.7554/eLife.36697; pmid: 30375975
18. A. Giuditta, W. D. Dettbarn, M. Brzin, Protein synthesis in the isolated giant axon of the squid. *Proc. Natl. Acad. Sci. U.S.A.* **59**, 1284–1287 (1968). doi: 10.1073/pnas.59.4.1284; pmid: 5242241
19. R. J. Lasek, C. Dabrowski, R. Nordlander, Analysis of axoplasmic RNA from invertebrate giant axons. *Nat. New Biol.* **244**, 162–165 (1973). doi: 10.1038/newbio244162a0; pmid: 4516445
20. M. R. Akins, H. E. Berk-Rauch, J. R. Fallon, Presynaptic translation: Stepping out of the postsynaptic shadow. *Front. Neural Circuits* **3**, 17 (2009). doi: 10.3389/neuro.04.017.2009; pmid: 19915727
21. R. D. Vale, T. S. Reese, M. P. Sheetz, Identification of a novel force-generating protein, kinesin, involved in microtubule-based motility. *Cell* **42**, 39–50 (1985). doi: 10.1016/S0092-8674(85)80099-4; pmid: 3926325
22. P. W. Tillberg *et al*., Protein-retention expansion microscopy of cells and tissues labeled using standard fluorescent proteins and antibodies. *Nat. Biotechnol.* **34**, 987–992 (2016). doi: 10.1038/nbt.3625; pmid: 27376584
23. E. Herzog *et al*., The existence of a second vesicular glutamate transporter specifies subpopulations of glutamatergic neurons. *J. Neurosci.* **21**, RC181 (2001). doi: 10.1523/JNEUROSCI.21-22-j0001.2001; pmid: 11698619
24. R. T. Fremeau Jr. *et al*., The expression of vesicular glutamate transporters defines two classes of excitatory synapse. *Neuron* **31**, 247–260 (2001). doi: 10.1016/S0896-6273(01)00344-0; pmid: 11502256
25. S. L. McIntire, R. J. Reimer, K. Schuske, R. H. Edwards, E. M. Jorgensen, Identification and characterization of the vesicular GABA transporter. *Nature* **389**, 870–876 (1997). doi: 10.1038/39908; pmid: 9349821
26. C. Sagné *et al*., Cloning of a functional vesicular GABA and glycine transporter by screening of genome databases. *FEBS Lett.* **417**, 177–183 (1997). doi: 10.1016/S0014-5793(97)01279-9; pmid: 9395291
27. E. Luquet, C. Biesemann, A. Munier, E. Herzog, Purification of Synaptosome Populations Using Fluorescence-Activated Synaptosome Sorting. *Methods Mol. Biol.* **1538**, 121–134 (2017). doi: 10.1007/978-1-4939-6688-2_10; pmid: 27943188
28. C. Biesemann *et al*., Proteomic screening of glutamatergic mouse brain synaptosomes isolated by fluorescence activated sorting. *EMBO J.* **33**, 157–170 (2014). doi: 10.1002/embj.201386120; pmid: 24413018
29. V. P. Whittaker, I. A. Michaelson, R. J. Kirkland, The separation of synaptic vesicles from nerve-ending particles ('synaptosomes'). *Biochem. J.* **90**, 293–303 (1964). doi: 10.1042/bj0900293; pmid: 5834239
30. E. Herzog *et al*., In vivo imaging of intersynaptic vesicle exchange using VGLUT1 Venus knock-in mice. *J. Neurosci.* **31**, 15544–15559 (2011). doi: 10.1523/JNEUROSCI.2073-11.2011; pmid: 22031900
31. A. Vukoja *et al*., Presynaptic Biogenesis Requires Axonal Transport of Lysosome-Related Vesicles. *Neuron* **99**, 1216–1232.e7 (2018). doi: 10.1016/j.neuron.2018.08.004; pmid: 30174114
32. J. C. Darnell *et al*., FMRP stalls ribosomal translocation on mRNAs linked to synaptic function and autism. *Cell* **146**, 247–261 (2011). doi: 10.1016/j.cell.2011.06.013; pmid: 21784246
33. E. K. Schmidt, G. Clavarino, M. Ceppi, P. Pierre, SUnSET, a nonradioactive method to monitor protein synthesis. *Nat. Methods* **6**, 275–277 (2009). doi: 10.1038/nmeth.1314; pmid: 19305406
34. G. M. Shepherd, K. M. Harris, Three-dimensional structure and composition of CA3–>CA1 axons in rat hippocampal slices: Implications for presynaptic connectivity and compartmentalization. *J. Neurosci.* **18**, 8300–8310 (1998). doi: 10.1523/JNEUROSCI.18-20-08300.1998; pmid: 9763474
35. S. tom Dieck *et al*., Direct visualization of newly synthesized target proteins in situ. *Nat. Methods* **12**, 411–414 (2015). doi: 10.1038/nmeth.3319; pmid: 25775042
36. H. Kang, E. M. Schuman, A requirement for local protein synthesis in neurotrophin-induced hippocampal synaptic plasticity. *Science* **273**, 1402–1406 (1996). doi: 10.1126/science.273.5280.1402; pmid: 8703078
37. K. M. Huber, J. C. Roder, M. F. Bear, Chemical induction of mGluR5- and protein synthesis—Dependent long-term depression in hippocampal area CA1. *J. Neurophysiol.* **86**, 321–325 (2001). doi: 10.1152/jn.2001.86.1.321; pmid: 11431513
38. J. Zhong, T. Zhang, L. M. Bloch, Dendritic mRNAs encode diversified functionalities in hippocampal pyramidal neurons. *BMC Neurosci.* **7**, 17 (2006). doi: 10.1186/1471-2202-7-17; pmid: 16503994
39. E. S. Lein *et al*., Genome-wide atlas of gene expression in the adult mouse brain. *Nature* **445**, 168–176 (2007). doi: 10.1038/nature05453; pmid: 17151600
40. M. M. Poon, S. H. Choi, C. A. Jamieson, D. H. Geschwind, K. C. Martin, Identification of process-localized mRNAs from cultured rodent hippocampal neurons. *J. Neurosci.* **26**, 13390–13399 (2006). doi: 10.1523/JNEUROSCI.3432-06.2006; pmid: 17182790
41. I. J. Cajigas *et al*., The local transcriptome in the synaptic neuropil revealed by deep sequencing and high-resolution imaging. *Neuron* **74**, 453–466 (2012). doi: 10.1016/j.neuron.2012.02.036; pmid: 22578497
42. L. F. Gumy *et al*., Transcriptome analysis of embryonic and adult sensory axons reveals changes in mRNA repertoire localization. *RNA* **17**, 85–98 (2011). doi: 10.1261/rna.2386111; pmid: 21098654
43. K. H. Zivraj *et al*., Subcellular profiling reveals distinct and developmentally regulated repertoire of growth cone mRNAs. *J. Neurosci.* **30**, 15464–15478 (2010). doi: 10.1523/JNEUROSCI.1800-10.2010; pmid: 21084603
44. L. A. Autilio, S. H. Appel, P. Pettis, P. L. Gambetti, Biochemical studies of synapses in vitro. I. Protein synthesis. *Biochemistry* **7**, 2615–2622 (1968). doi: 10.1021/bi00847a025; pmid: 5660078
45. I. G. Morgan, L. Austin, Synaptosomal protein synthesis in a cell-free system. *J. Neurochem.* **15**, 41–51 (1968). doi: 10.1111/j.1471-4159.1968.tb06172.x; pmid: 4230127
46. S. Maday, A. E. Twelvetrees, A. J. Moughamian, E. L. Holzbaur, Axonal transport: Cargo-specific mechanisms of motility and regulation. *Neuron* **84**, 292–309 (2014). doi: 10.1016/j.neuron.2014.10.019; pmid: 25374356
47. S. J. Tang *et al*., A rapamycin-sensitive signaling pathway contributes to long-term synaptic plasticity in the hippocampus. *Proc. Natl. Acad. Sci. U.S.A.* **99**, 467–472 (2002). doi: 10.1073/pnas.012605299; pmid: 11756682
48. M. A. Sutton *et al*., Miniature neurotransmission stabilizes synaptic function via tonic suppression of local dendritic protein synthesis. *Cell* **125**, 785–799 (2006). doi: 10.1016/j.cell.2006.03.040; pmid: 16713568
49. J. D. Richter, G. J. Bassell, E. Klann, Dysregulation and restoration of translational homeostasis in fragile X syndrome. *Nat. Rev. Neurosci.* **16**, 595–605 (2015). doi: 10.1038/nrn4001; pmid: 26350240
50. M. R. Akins *et al*., Axonal ribosomes and mRNAs associate with fragile X granules in adult rodent and human brains. *Hum. Mol. Genet.* **26**, 192–209 (2017). pmid: 28082376
51. K. M. Huber, M. S. Kayser, M. F. Bear, Role for rapid dendritic protein synthesis in hippocampal mGluR-dependent long-term depression. *Science* **288**, 1254–1256 (2000). doi: 10.1126/science.288.5469.1254; pmid: 10818003
52. W. B. Smith, S. R. Starck, R. W. Roberts, E. M. Schuman, Dopaminergic stimulation of local protein synthesis enhances surface expression of GluR1 and synaptic transmission in hippocampal neurons. *Neuron* **45**, 765–779 (2005). doi: 10.1016/j.neuron.2005.01.015; pmid: 15748851
53. G. Tushev *et al*., Alternative 3′ UTRs modify the localization, regulatory potential, stability, and plasticity of mRNAs in neuronal compartments. *Neuron* **98**, 495–511.e6 (2018). doi: 10.1016/j.neuron.2018.03.030; pmid: 29656876
54. G. Aakalu, W. B. Smith, N. Nguyen, C. Jiang, E. M. Schuman, Dynamic visualization of local protein synthesis in hippocampal neurons. *Neuron* **30**, 489–502 (2001). doi: 10.1016/S0896-6273(01)00295-1; pmid: 11395009
55. A. S. Hafner *et al*., Lengthening of the stargazin cytoplasmic tail increases synaptic transmission by promoting interaction to deeper domains of PSD-95. *Neuron* **86**, 475–489 (2015). doi: 10.1016/j.neuron.2015.03.013; pmid: 25843401
56. C. Fallini, P. G. Donlin-Asp, J. P. Rouanet, G. J. Bassell, W. Rossoll, Deficiency of the survival of motor neuron protein impairs mRNA localization and local translation in the growth cone of motor neurons. *J. Neurosci.* **36**, 3811–3820 (2016). doi: 10.1523/JNEUROSCI.2396-15.2016; pmid: 27030765
57. C. C. Chou *et al*., TDP-43 pathology disrupts nuclear pore complexes and nucleocytoplasmic transport in ALS/FTD. *Nat. Neurosci.* **21**, 228–239 (2018). doi: 10.1038/s41593-017-0047-3; pmid: 29311743
58. Genome Reference Consortium Mouse Build 38, mm10 (2011); http://hgdownload.soe.ucsc.edu/goldenPath/mm10/bigZips/.
59. A. Dobin *et al*., STAR: Ultrafast universal RNA-seq aligner. *Bioinformatics* **29**, 15–21 (2013). doi: 10.1093/bioinformatics/bts635; pmid: 23104886
60. Genomics Institute, UCSC, Table Browser; http://genome.ucsc.edu/cgi-bin/hgTables?hgsid=706713641_R7J6gGZbwmO18wecxAAiXglgAlzN&clade=mammal&org=Mouse&db=mm10&hgta_group=genes&hgta_track=refSeqComposite&hgta_table=0&hgta_regionType=genome&position=chr12%3A56694976-56714605&hgta_outputType=primaryTable&hgta_outFileName=.
61. Walter and Eliza Hall Institute, featureCounts: a ultrafast and accurate read summarization program; http://bioinf.wehi.edu.au/featureCounts/.
62. Bioconductor, DESeq2; https://bioconductor.org/packages/release/bioc/html/DESeq2.html.
63. D. J. McCarthy, Y. Chen, G. K. Smyth, Differential expression analysis of multifactor RNA-Seq experiments with respect to biological variation. *Nucleic Acids Res.* **40**, 4288–4297 (2012). doi: 10.1093/nar/gks042; pmid: 22287627
64. Y. Benjamini, Y. Hochberg, Controlling the false discovery rate: A practical and powerful approach to multiple testing. *J. R. Stat. Soc. B* **57**, 289–300 (1995). doi: 10.1111/j.2517-6161.1995.tb02031.x
65. W. J. Kent, BLAT—The BLAST-like alignment tool. *Genome Res.* **12**, 656–664 (2002). doi: 10.1101/gr.229202
66. J. C. Oliveros, (2015). Venny. An interactive tool for comparing lists with Venn's diagrams; http://bioinfogp.cnb.csic.es/tools/venny/index.html.

ACKNOWLEDGMENTS

We thank I. Bartnik, N. Fuerst, A. Staab, D. Vogel, and C. Thum for the preparation of cultured neurons; S. tom Dieck and T.W. Lee for important work in preliminary studies; H. Nguyen for experiments shown in Fig. 4H and fig. S7B; M. F. Angelo, A. Stum, and V. Pitard (flow cytometry facility, CNRS UMS 3427, INSERM US 005, University of Bordeaux, F-33000 Bordeaux, France) for technical assistance with FASS experiments; F. Cordelières (Bordeaux Imaging Center, University of Bordeaux, F-33000 Bordeaux, France) for image analysis routines; and G. Tushev for help with RNA sequencing analyses. **Funding:** A.-S.H. is supported by an EMBO long-term postdoctoral fellowship (ALTF 1095-2015) and the Alexander von Humboldt Foundation (FRA-1184902-HFST-P), as well as the National Infrastructure France–BioImaging, supported by the French National Research Agency (ANR-10-INBS-04). P.G.D.-A. is supported by the Peter and Traudl Engelhorn Foundation and the Alexander von Humboldt Foundation (USA-1198990-HFST-P). E.M.S. is funded by the Max Planck Society, an Advanced Investigator award from the European Research Council, DFG CRC 1080: Molecular and Cellular Mechanisms of Neural Homeostasis, and DFG CRC 902: Molecular Principles of RNA-based Regulation. This project has received funding from the European Research Council (ERC) under the European Union's Horizon 2020 research and innovation program (grant agreement 743216). B.L. is funded by the Royal Society NZ–Germany Science and Technology Programme (FRG-UOO1403). E.H. is funded by the French National Research Agency (ANR-10-LABX-43 BRAIN Dolipran) and the Fondation pour la Recherche Médicale (ING20150532192). **Author contributions:** A.-S.H. and P.G.D.-A. designed, conducted, and analyzed experiments. E.H. and B.L. designed and supervised experiments. E.M.S. designed experiments, supervised the project, and wrote the paper. All authors edited the paper. **Competing interests:** The authors declare no competing financial interests. **Data and materials availability:** All data are available in the main text or the supplementary materials. The accession number for the raw sequencing data reported in this paper is NCBI BioProject: PRJNA544779.

SUPPLEMENTARY MATERIALS

science.sciencemag.org/content/364/6441/eaau3644/suppl/DC1
Figs. S1 to 13
Tables S1 and S2
Movie S1

3 June 2018; resubmitted 16 January 2019
Accepted 2 April 2019
10.1126/science.aau3644

Local protein synthesis is a ubiquitous feature of neuronal pre- and postsynaptic compartments

Anne-Sophie HafnerPaul G. Donlin-AspBeulah LeitchEtienne HerzogErin M. Schuman

Science, 364 (6441), eaau3644. • DOI: 10.1126/science.aau3644

Local translation in presynaptic terminals

Proteins carry out most of the functions in cells, including neurons, which are one of the most morphologically complex cell types in the body. This poses challenges for how proteins can be supplied to remote regions where connections (synapses) are made with other neurons. One solution to the neuron protein-supply problem involves the local synthesis of proteins from messenger RNA (mRNA) molecules located at or near synapses. Hafner *et al.* used RNA sequencing methods and superresolution microscopy to show that axon terminals contain hundreds of mRNA molecules as well as the machinery needed for protein synthesis. Furthermore, the axon terminals were able to use these components to make proteins that participate in synaptic transmission.

Science, this issue p. eaau3644

Science (ISSN 1095-9203) is published by the American Association for the Advancement of Science. 1200 New York Avenue NW, Washington, DC 20005. The title *Science* is a registered trademark of AAAS.